# Doppler-free Rb saturation Spectroscopy

Julia Latour

August 2023

## Contents

# 1 Introduction

In this experiment, we investigate the absorption and saturation spectra of Rubidium by means of Doppler-free laser spectroscopy. The main goal is to focus on the ground state properties of the hyperfine structure characteristic to isotopes $^{8}7Rb$ and $^{8}5Rb$, as well as the transitions to the excited states. In the first part, the key topics are shortly introduced. The second part involves the results and discussion.

## 1.1 Natural line width

Molecules with no external interactions exist in a ground state- configuration minimizing their total energy. Atoms, either tied up in a molecule or on their own, above the ground state, have a discrete energy levels spectrum. Each of those levels can be reached upon excitation via absorption of electromagnetic radiation of adequate wavelength or colliding with other excited molecules. The higher energy levels are unstable, thus excited atoms quickly return to the lower or ground energy state. It takes them $\tau_{rel}$ known as 'relaxation time' to do so.

Returning to a more stable state corresponds to re-emission of the electromagnetic radiation. A close model of a harmonic oscillator allowing us to describe the behavior of molecules in a dipole antenna. The energy loss in the process is described by oscillation's attenuation, i.e. damping with a $\gamma$ constant. Moreover, a k spring constant and mass of an excited electron $m_e$ make up a resonant frequency of $\omega_0^2 = \frac{k}{m_e}$. In the end, we can write the equation of motion:

$$\ddot{x} + \gamma\dot{x} + \omega_0^2 x = 0 \tag{1}$$

We further care about the real solution, obtained with initial values x(0)=$x_0$ and $\dot{x}(0) = 0$:

$$x(t) = x_0 e^{-(\gamma/2)t}[\cos\omega t + \frac{\gamma}{2\omega}\sin\omega t] \tag{2}$$

After introducing an approximation for small damping ($\gamma$ much smaller than $\omega_0$), it is set that $\omega \approx \omega_0$ and the sin term is neglected, as reads in [1](eq. 3.5), such that;

$$x(t) = x_0 e^{-(\gamma_0/2)t}[\cos\omega_0 t] \tag{3}$$

If we consider two atomic energy levels $E_i$ and $E_k$, the central frequency $\omega_{ik} = (E_i - E_k)/\hbar$ corresponds to $\omega_0 = 2\pi\nu_0$ [1].

Because of the damped character of the oscillation, the amplitude decreases making the emitted radiation's frequency non-monochromatic. It can now be described by a Fourier transform- superposition of monochromatic oscillations of different amplitudes and frequencies.

$$A(\omega) = \frac{1}{\sqrt{2\pi}}\int_{-\infty}^{+\infty} x(t)e^{-i\omega t}dt \tag{4}$$

$$A(\omega) = \frac{1}{\sqrt{2\pi}}\int_{0}^{+\infty} x_0 e^{(\frac{-\gamma t}{2})}\cos(\omega_0 t)e^{-i\omega t}dt \tag{5}$$

Then, the inverse Fourier transform will give us a new expression of x(t):

$$x(t) = \frac{1}{\sqrt{2\pi}}\int_0^\infty A(\omega)\cdot e^{i\omega t}d\omega$$

The intensity distribution can be further calculated after determining explicitly $A(\omega)$ with the analytical solution, since $I(\omega) \propto A(\omega)A*(\omega)$. From [1]:

$$I(\omega - \omega_0) = \frac{C}{(\omega-\omega_0)^2 + (\frac{\gamma}{2})^2} \tag{6}$$

With $C = \frac{I_0\gamma}{2\pi}$ by normalisation. Moving forward, we normalise the line profile $I(\omega)$, resulting in a so-called 'normalised Lorentzian profile':

$$g(\omega) = \frac{\frac{\gamma}{2\pi}}{(\omega-\omega_0)^2+(\frac{\gamma}{2})^2}$$

The FWHM (full width a half maximum) of this profile is precisely the natural line width $\delta\omega_n$.

The profile's maximum is located at the resonance frequency $\omega_0$, where $g(\omega_0) = \frac{\gamma}{2\pi}(\frac{2}{\gamma})^2 = \frac{2}{\gamma\pi}$. From $g(\omega_0 + \frac{\delta\omega_n}{2}) = \frac{1}{\gamma\pi}$ it follows that:

$$\delta\omega_n = \gamma\delta\nu_n = \frac{\gamma}{2\pi} \tag{7}$$

Lastly, it is possible to relate the FWHM to the lifetime of an excited state through $\frac{\delta_n}{2\pi} = \frac{1}{\tau}$. After the lifetime, the emitted intensity has dropped to $\frac{1}{e}$ [2](Page 7).

The introduction of a Lorentzian line profile approximation constitutes a broadening effect, as it produces a distribution of intensities as a solution instead of a single value.

## 1.2 Doppler broadening effect

Usually, other broadening effects completely outrule the Lorentzian line profile, influencing the spectral linewidth.

Since the measurements are not performed at temperatures close to absolute zero, the thermal motion of the molecules (emitting or absorbing) also plays a role in a low-pressure constraint. Such a set of particles in an enclosed space should follow the Maxwell-Boltzmann distribution. Secondly, the Doppler effect will influence the absorbed and emitted frequencies.

If we consider an emitting molecule moving with velocity $v$, observed against the direction of 'k', the wave vector of the emitted radiation, then its emitted frequency from the observer's perspective changes to:

$$\omega_e = \omega_0 + \vec{k} \cdot \vec{v} \tag{8}$$

Hence, if the second term is positive (molecule moving towards the observer), the total emitted frequency will increase, and the opposite for a negative term (molecule moving away from the observer). An absorbing molecule moving across a plane wave with velocity v, in its rest frame will see the wave frequency as:

$$\omega' = \omega - \vec{k} \cdot \vec{k} \tag{9}$$

For the molecule to absorb, the radiation has to be equal to its eigenfrequency $\omega_0$, which results in:

$$\omega_a = \omega_0 + \vec{k} \cdot \vec{v} \tag{10}$$

Now, the second summand will be either positive (molecule moving parallel to the wave propagation) or negative (molecule moving against the wave propagation). For a choice $\vec{k} = 0, 0, k_z$ and $|k| = \frac{2\pi}{\lambda}$:

$$\omega_a = \omega_0(1 + \frac{v_z}{c}) \tag{11}$$

Following the earlier comment about distribution, the probability that a particular state is occupied proportionally depedent on $e^{\frac{-mv^2}{2k_BT}}$. The velocity probability distribution is equal to [1](eq. 11):

$$p(v)dv = p(v)dv = 4\pi\Big(\frac{m}{2k_BT\pi}\Big)^{\frac{3}{2}} v^2 e^{\frac{-mv^2}{2k_BT}} dv \tag{12}$$

On the way of simplification, we can consider just one component of the most probable velocity found by $\frac{\partial p(v)}{\partial v} \stackrel{!}{=} 0$ ($v_p = \sqrt{\frac{2k_BT}{m}}$) as v [2](eq. 13):

$$p(v_z)dv_z = \sqrt{\frac{m}{2k_BT\pi}} \cdot e^{\frac{-mv_z^2}{2k_BT}} dv_z = \frac{1}{v_p\sqrt{\pi}} \cdot e^{-(\frac{v_z}{v_p})} dv_z \tag{13}$$

At thermal equilibrium, the number density of molecules $n_i(v_z)dv_z$ with energy $E_i$ and velocity component in the range $[v_z, v_z + dv_z]$ is [1]:

$$n_i(v_z)dv_z = \frac{N_i}{v_p\sqrt{\pi}} e^{-(\frac{v_z}{v_p})^2} dv_z \tag{14}$$

In the experiment, we can only measure the distribution as a function of radiation frequency (absorbed or emitted). Therefore, we change the number density to an expression in $\omega$ by calculating $v_z = c(\frac{\omega}{\omega_0} - 1)$ and $dv_z = \frac{c}{\omega_0} d\omega$ from equation (number of the equation for doppler shifted frequency). Finally, the transformed number density is:

$$n_i(\omega)d\omega = \frac{N_i c}{v_p\omega_0\sqrt{\pi}} \frac{c}{\omega_0} \cdot e^{-c^2\left(\frac{\omega-\omega_0}{v_p\omega_0})\right)^2} \tag{15}$$

Now, the intensity profile is different from the previously discussed Lorentzian. We know that the intensity distribution should be proportional to the number density $n_i(\omega)$. Hence we obtain the expression called the **Gauss profile**:

$$I(\omega) = I(\omega_0) e^{-\left(\frac{\omega-\omega_0}{\omega_0 \frac{v_p}{c}}\right)^2} \tag{16}$$

The FWHM is:

$$\delta\omega_D = \frac{\omega_0}{c}\sqrt{\frac{k_BTln(2)}{m}} \tag{17}$$

As it can be shown in experimental examples [2](Page 9) the $\delta\omega_D$ is much higher than the natural line

width, as the broadening grows proportionally to the eigenfrequency.

What is left is to consider the Lorentzian profile each molecule has at different central frequencies due to the finite time of emission, as not all molecules with a velocity component $v_z$ absorb/emit at the same frequency. This is done by creating a third, Voigt profile– a convolution of the Lorenzian and Doppler-Gaussian profiles:

$$I(\omega) = \frac{\gamma I_0 N_i c}{2\pi^{\frac{3}{2}}\omega_0 v_p} \int \frac{e^{-c^2\frac{\omega-\omega_0)^2}{(\omega_0 v_p)^2}}}{(\omega-\omega_0)^2 + (\frac{\gamma}{2})^2} \tag{18}$$

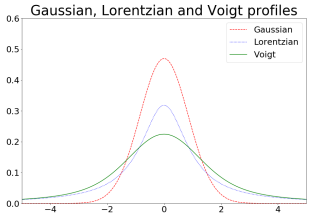


Figure 1: The three profiles. (Common media)

### 1.2.1 Homogeneous and inhomogeneous line broadening

A spectral line profile is called homogeneously broadened if the probability $P_{ik}(\omega)$ of absorption/emission of radiation of $\omega$ frequency allowing for transition between states $|i\rangle \Rightarrow |k\rangle$ is equal for all molecules found at state $|i\rangle$. An example is the normalised Lorentzian profile $g(\omega - \omega_0)$, with the probability equal for all molecules in level $E_i$, expressed by:

$$P_{ik}(\omega) = A_{ik} g(\omega - \omega_0)$$

where $A_{ik}$ is the Einstein coefficient of spontaneous emission.

If the probability, as earlier defined is not the same for all molecules at state $|i\rangle$, the profile is called heterogeneously broadened. The heterogeneous broadening is a characteristic of the Doppler broadening, as molecules in the same energy level can possess different reference point-relative velocities making up different Gaussian lie profiles and hence different absorption/emission probabilities.

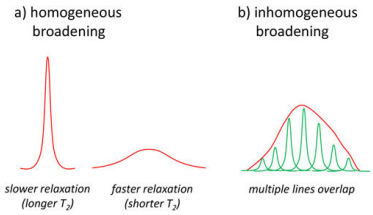


Figure 2: Inhomogeneous and homogeneous profile. Adapted from [6]

## 1.3 Saturation by Optical Pumping

Optical pumping is achieved by consideration of a two-level system of two population densities $N_1$ and $N_2$. These two levels are exclusively (no other levels come into the interactions) connected by absorption/emission or relaxation processes. If we now define the probability P of transition between the two nondegenerate levels with statistical weight factors $g_i = 1$ (via absorption or emission) and relaxation probabilities $R_1$ ad $R_2$, we can write a rate equation for the level population:

$$\frac{dN_1}{dt} = -\frac{dN_2}{dt} = 0 = -PN_1 - R_1 N_1 + PN_2 + R_2 N_2$$

With $N_1 + N_2 = N$:

$$N_1 = N\frac{P+R_2}{2P+R_1+R_2}, \quad N_2 = N\frac{P+R_1}{2P+R_1+R_2}$$

For P much larger than $R_i$, the limits of both populations are equal to N/2, which means that both levels become equally populated. Then, the medium becomes transparent, as the absorption coefficient proportional to the difference between levels' populations is zero. Assuming no external radiation, the pumping rate P=0 and the new equilibrium gives:

$$N_{10} = \frac{R_2}{R_1+R_2}N, \quad N_{20} = \frac{R_1}{R_1+R_2}N$$

After introducing $\Delta N = N_1 - N_2$ and $\Delta N_0 = N_{10} - N_{20}$, we obtain:

$$\Delta N = \frac{\Delta N_0}{1+2P/(R_1+R_2)} = \frac{\Delta N_0}{1+S}$$

$$S = \frac{2P}{R_1+R_2} = \frac{P}{\overline{R}} \text{ where } \quad \overline{R} = \frac{R_1+R_2}{2}$$

$\overline{R}$ is known as the average relaxation rate. Thus, S defined as the 'saturation parameter', is a ratio of the pumping rate and the average relaxation rate. With the assumption of a monochromatic wave used for pumping [1](Page 91), the rate P equals:

$$P = \sigma_{12}(\omega)\frac{I(\omega)}{h\bar{\omega}}$$

Then, by assuming the emission from the upper (2) level is the only possible relaxation, $R_1 = 0$ and $R_2 = A_{21}$. Eventually, it leads us to a new expression for the saturation parameter:

$$S = \frac{2\sigma_{12}I(\omega)}{\hbar\omega A_{21}}$$

Where:

$$\alpha(\omega) = \sigma_{12}\Delta N$$

is the saturated absorption coefficient, otherwise expressed with the unsaturated absorption coefficient $\alpha_0$ and absorption cross-section of the molecules $\sigma 12$ as:

$$\alpha = \frac{\alpha_0}{1+S}$$

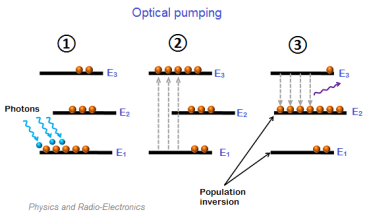


Figure 3: Optical pumping. Adapted from [7]

## 1.4 Linear and nonlinear absorption

Exclusive saturation of a chosen transition gradually makes the population of a lower, absorbing level smaller. In the further discussion, we will try to describe a $|i\rangle \Rightarrow |k\rangle$ By considering various additional influences, such as collisions, diffusion of molecules into/out of excitation volume, or fluorescence, total stationary population density can be defined with emptying and filling rates. For various cases, we find different expressions for the population densities, which later can be substituted into the expression for absorbed power in volume Adx:

$$dP = AI\sigma ik\Big[N_i - \frac{g_i}{g_k}N_k\Big]dx$$

In a low-intensity regime, by analyzing a limiting case (I=0), we can see that the thermal population density is a ratio of filling to emptying rate, which is constant. Hence, the absorbed power expression, after substituting $N_i$ is approximately linear in I. In our experiment, however, a coherent, laser light source will be used, belonging to the high-intensity regime. As presented in [2](Page 14), in this case, the population density solution is already linear in I, making the absorbed power show both linear and quadratic dependence of its terms:

$$dP \approx A \cdot \sigma_{ik} \cdot N_i^0\Big(I - \frac{B_{ik}}{c\gamma_i}I^2\Big)dz \tag{19}$$

Here, again the $\sigma_{ik}$ is the absorption cross-section, the $B_{ik}$ is the Einstein coefficient for absorption, and the z increment denotes the displacement of incident light in the absorbing material of area A.

In a very high-intensity regime, the populations of the two levels become equal. Moreover, as I$\Rightarrow \infty$ the absorption coefficient reaches 0, as the sample becomes fully transparent [2](Page 14).

The saturation parameter is introduced with:

$$N_i = \frac{N_i^0}{1+S_i} \text{ and } S_i = \frac{B_{ik}I}{c\gamma_i}$$

The overall saturation of a substance relies on the transition $|i\rangle \Rightarrow |k\rangle$ saturation, described by the coefficient of transition:

$$S_{ik} = \frac{2B_{ik}I}{c}\left[\frac{1}{\gamma_i} + \frac{1}{\gamma_k}\right] \tag{20}$$

Next, one can find a 'saturation intensity', at which $S_{ik} = 1$. For $S \ll 1$ and homogeneous line broadening the following population densities are found:

$$N_i(\omega) = N_i^0 - \frac{\Delta N^0}{\gamma_i\tau}\frac{S_0(\frac{\gamma}{2})^2}{(\omega-\omega_0)^2+(\frac{\gamma}{2})^2}$$
$$N_k(\omega) = N_k^0 + \frac{\Delta N^0}{\gamma_k\tau}\frac{S_0(\frac{\gamma}{2})^2}{(\omega-\omega_0)^2+(\frac{\gamma}{2})^2}$$

where $\tau = \frac{\gamma}{\gamma_i\gamma_k}$, $\gamma = \gamma_i + \gamma_k$ being the transition line width, $\Delta N^0 = N_i^0 - N_k^0$ is the difference in thermal populations for 0 saturation.

## 1.5 Saturation broadening of homogeneously broadened transitions

A homogeneously broadened transition has the pumping rate $P(\omega)$ with a Lorentzian profile, thus its frequency-dependent saturation parameter $S(\omega) = \frac{P}{R}$ has the same profile.

$$S_\omega = S - 0\frac{\gamma/2)^2}{(\omega-\omega_0)^2+(\gamma/2)^2} \text{ with } S_0 = S_\omega$$

Later, a calculation of the power absorbed for transition to the energetically higher level allows us to find an expression for a frequency-dependent absorption coefficient.

$$\alpha_s(\omega) = \alpha_0(\omega_0)\frac{(\frac{\gamma}{2})^2}{(\omega-\omega_0)^2+(\frac{\gamma_s}{2})^2} = \frac{\alpha_0(\omega)}{1+S_\omega}$$

also characterized by the Lorentzian profile. This time, for the saturation case the line width has increased compared to $\gamma$, the line width for transition with no saturation:

$$\gamma_s = \gamma \cdot \sqrt{1 + S(\omega_0)}$$

Now we want to compare the saturated to unsaturated absorption profile. The formula for the latter is:

$$\alpha_0(\omega) = \frac{\alpha_0(\omega_0)(\gamma/2)^2}{(\omega-\omega_0)^2+(\gamma/2)^2}$$

By comparison between the two cases, we notice that in saturation the absorption coefficient is decreased by the factor of $(1 + S_\omega)$. Since $S_\omega$ has a maximum at the eigenfrequency of transition and tends to 0 for both larger and smaller frequencies, the compression of the absorption coefficient will be the largest at the eigenfrequency and smallest further away from the $\omega_0$, where $S_\omega = 1$ at infinities.

## 1.6 Saturation broadening of inhomogeneously broadened transitions

This time we will consider an example of inhomogeneous broadening, i.e. Doppler broadening. In the two expressions for saturated population densities obtained before for homogeneous broadening, we substitute the Doppler-shifted frequencies, yielding:

$$N_i(\omega, v_z) - N_i^0(v_z) - \frac{\Delta N^0}{\gamma_i \tau}\frac{S_0(\frac{\gamma}{2})^2}{(\omega-\omega_0-kv_z)^2+(\frac{\gamma_s}{2})^2}$$
$$N_k(\omega, v_z) = N_k^2(v_z) + \frac{\Delta N^0}{\gamma_k \tau}\frac{S_0(\frac{\gamma}{2})^2}{(\omega-\omega_0-kv_z)^2+(\frac{\gamma_s}{2})^2}$$

Next, a difference in the two population densities can be found:

$$\Delta N(\omega, v_x) = \Delta N^0(v_x)\left(1 - \frac{S_0(\frac{\gamma}{2})^2}{(\omega-\omega_0-kv_x)^2+(\frac{\gamma_s}{2})^2}\right)$$

There is a hole in the distribution (difference) under the name of a 'Bennet hole' It arises as both levels: absorption (lower) and emission (higher) have respectively a minimum and maximum at the point $v_x = (\omega - \omega_0)/k$. To indirectly measure the population densities, one needs to evaluate the absorption coefficient, the measured intensity is proportional to:

$$\alpha(\omega) = \int \Delta N(v_x)\sigma(\omega, v_x)dv_x$$

With $\sigma(\omega, v_z)$ being the optical absorption cross-section of the molecule. After putting in all the precise formulas for the factors, as the unsaturated Doppler-broadening, a Voigt profile is achieved:

$$\alpha(\omega) = \frac{\Delta N^0 \sigma_0}{v_p \pi}\int \frac{\exp\left(\frac{v_x}{v_p}\right)^2}{(\omega-\omega_0-kv_x)^2+\left(\frac{\gamma_s}{2}\right)^2}$$

## 1.7 Saturation Spectroscopy

The previously obtained expression for the absorption coefficient does not, however, carry the information about the bennet hole- there is no hole in its saturated distribution. That would mean that with the available means, the hole cannot be measured. The saturation spectroscopy introduces two anti-colinear laser beams- a probe beam with small intensity and a pump beam with a much larger intensity compared to the latter. While the probe beam is of a fixed frequency, causing a Bennet hole (hole burning) in the population densities difference for a restricted velocity interval. The probe beam varies in frequency according to the Doppler distribution. With the two beams shone, the absorption coefficient is the following:

$$\alpha_s(\omega) =$$
$$\alpha^0(\omega)\left(a - \frac{S_0}{\sqrt{1+S_0}}\frac{(\frac{\gamma}{2})^2}{(\omega-\omega_0-kv_x)^2+(\frac{\gamma[1+(1+S_0)^{0.5}]}{2})^2}\right)$$

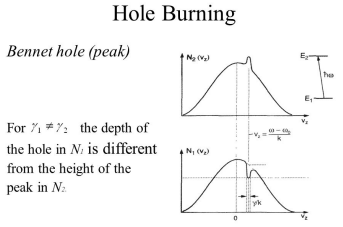


Figure 4: Hole burning. Adapted from [https://slideplayer.com]

The $\alpha_S(\omega)$ has a Gauss profile with a local minimum in the center- the 'Lamb dip'. Depending on the frequency of the pump beam, molecules with distinct velocities with respect to the beam will trigger the absorption. For the probe beam, the same will happen for molecules moving in the opposite direction to the pump beam. If the frequency of the pump beam does not match the eigenfrequency of absorption, molecules of the non-triggering velocity components will be saturated. They will not, however, match the velocity components needed for absorption of the probe beam. The matching of velocities, i.e. the same group of atoms/molecules will absorb both beams if the frequency of the beams is equal to the eigenfrequency, $\omega_0$. The group of molecules will be specifically those that move perpendicularly to the axis of the beams or are not moving at all. At $\omega_0$, the higher energy level becomes saturated enough for the sample to become transparent. Then, the probe beam can pass to the detector nearly not affected. That is when the absorption profile will encounter a drop, causing the Lamb dip. All in all, if we first try out a spectrum of frequencies on the sample (the pump beam), we will cut out a hole in the absorption profile by saturating the higher level. Then, the probe beam will serve as the analysis tool, checking the specific value of $\omega_0$.

## 1.8 Fine structure

The interaction between the orbital and spin angular momentum of an electron causes a rise of an extra contribution to the Hamiltonian. The contribution is proportional to the product of the two quantities: $\vec{L}$ and $\vec{S}$. A new quantity- the total angular momentum $\vec{J} = \vec{S} + \vec{J}$ commutes now with the total Hamiltonian. The corresponding quantum number now will be j and the projection $j_z$, and $|l - s| \geq j \geq |l + s|$. Rubidium with the electronic configuration $[Kr]5s^1$ in the ground state, which makes up a $5^2S_{\frac{1}{2}}$ state term (l=0, $s = \frac{1}{2}$,$j = \frac{1}{2}$). The first excited states will correspond to the transition of the valency electron from s to p subshell, changing the l value from 0 to 1. That gives two possible j values: $j = \frac{1}{2}$ and $j = \frac{3}{2}$, resulting respectively in $5^2P_{\frac{1}{2}}$ and $5^2P_{\frac{3}{2}}$ state terms signaling two separate energy levels. Hence, we will have two distinct transition lines:

$$D_1 : 5^2S_{\frac{1}{2}} \Rightarrow 5^2P_{\frac{1}{2}} \ \nu_{D_1} = 377.1THz$$
$$D_2 : 5^2S_{\frac{1}{2}} \Rightarrow 5^2P_{\frac{3}{2}} \ \nu_{D_2} = 384.2THz$$

In the experiment, we will focus on the $D_2$ line.

## 1.9 Hyperfine structure

The nucleus also possesses an intrinsic angular momentum $\vec{I}$, which similarly to the case of fine splitting, interacts with the orbital angular momentum creating yet another contribution term of the Hamiltonian. For commutation reasons, there is another change in the relevant quantum number. This time, the quantity of the full sum of angular momenta $F \rightleftarrows \vec{J} + \vec{I}$ and its related f: $|j - i| \geq |j + i|$ are now considered. The naturally occurring mixture of rubidium isotopes of rubidium is 72.2% $^{85}Rb$ and 27.8% $^{87}Rb$. Different isotopes are characterized by different intrinsic angular momenta due to characteristic numbers of protons in their nuclei. Hence, $^{85}Rb$ has $i = \frac{3}{2}$, while the $^{87}Rb$ has $i = \frac{5}{2}$. Due to fine splitting, we end up with the energy levels:

ground state:

$$^{85}Rb \ : \ j = \tfrac{1}{2} \Rightarrow i = \tfrac{3}{2}, f = 1, 2$$
$$^{87}Rb \ : \ j = \tfrac{1}{2} \Rightarrow i = \tfrac{5}{2}, f = 2, 3$$

excited state:

$$^{85}Rb \ : \ j = \tfrac{1}{2} \Rightarrow i = \tfrac{3}{2}, f = 1, 2$$
$$^{85}Rb \ : \ j = \tfrac{3}{2} \Rightarrow i = \tfrac{3}{2}, f = 0, 3$$
$$^{87}Rb \ : \ j = \tfrac{1}{2} \Rightarrow i = \tfrac{5}{2}, f = 2, 3$$

$$^{87}Rb \ : \ j = \frac{3}{2} \Rightarrow i = \frac{5}{2}, f = 1, 4$$

## 1.10 Laser diode

### 1.10.1 Introduction: semiconductors

Semiconductors are usually solids with temperature-dependent conductive properties falling between those of a conductor and an insulator. They are characterized by an energy levels spectrum called the 'band structure'. The energy levels lay close to each other forming a quasi-continuous band structure. There is a valence (lower energy) and a conductive (higher energy) band with a band gap in between, a region of forbidden energy levels. In the middle of the band lays a line of Fermi Energy, indicating the border between the fully empty conduction band and a fully filled valence band at absolute zero.

## 1.11 Doping

Doping is a method of replacement of a semiconducting lattice atom with another atom with a different number of valency electrons. If the introduced replacement has fewer valency electrons compared to the original atom, we call the impurity an acceptor, and the semiconductor- 'p-doped'. In the opposite case, the impurity, the donor, has more valency electrons, and the semiconductor becomes 'n-doped'. The former type of impurity produces a hole, an equivalent of a positive charge influenced by the lattice's periodic potential. N-doping can raise the fermi energy between the energy level of the donor atom and the conduction band. Then, with thermal influence, the donated electron can be excited higher up in the conducting band, increasing the free-charge carrier concentration and the overall conductivity of the lattice.

$$\alpha = \frac{\alpha_0}{1+S}$$

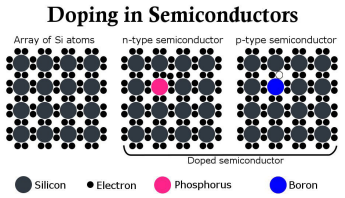


Figure 5: Doping example - silicon semiconductor. Adapted from [https://www.iceeet.com]

## 1.12 p-n junction without external voltage

Upon joining an n-doped and a p-doped region together, diffusion of the free charge carriers takes place creating recombination of the charges in the junction. In the end, a stripe of two regions with no free charge carriers arises between the n and p regions. The n remaining charges on the sides of the p and n doping will be the bound charges in the respective regions. Potential arising from the bound charges will prohibit further diffusion from the doped regions. With strong enough doping, the p-region's fermi level will be in the valence band while the region's fermi level will be located in the conductive band.

## 1.13 p-n junction with external voltage

Under the external voltage, a p-n junction forms a diode- an element letting through a current in a chosen direction and blocking the flow in the opposite. If the applied voltage direction supports a 'forward bias', the charges pass the diode and are conducted further into the circuit. If the voltage is applied in the opposite direction, it supports a 'reverse bias', where the passing charges encourage further recombination, widening the charge-carrier-free region and growth of the potential barrier.

$$\alpha = \frac{\alpha_0}{1+S}$$

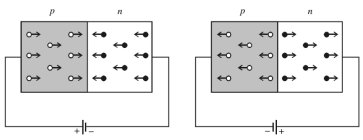

Figure 6: Forward and reverse bias - diode. Adapted from [https://www.studypage.in/]

## 1.14 Laser diode

Now we will consider an optical excitation by absorption of a photon with a wavelength corresponding to a transition (or slightly larger), electron-hole pairs are generated in both valence and conductive bands. A hole from the valence band can recombine with an electron from the conductive band releasing a photon of energy of the energy difference between the two quasi-particles: a hole and an electron. This effect is called the spontaneous emission. For the laser to work, stimulated emission is needed. A radiation field excites the recombination of hole-electron pairs by photons of a suitable wavelength. The recombination produces a photon of the same wavelength, direction, and phase as the stimulating photon. Since the stimulated and spontaneous emission always happens simultaneously. For lasing, the spontaneous must be largely outweighed by the stimulated emission. That requires building the laser as an 'optical resonator'. an area bounded by two mirrors and whose length L fulfills the condition of constructive interference. Emitted photons might become absorbed right away, making the progressive 'multiplication' of photons impossible. Thus, we need the 'gain'- the difference between spontaneous emission and absorption to be as large as possible. For the gain to be positive, population inversion is needed: the number of electrons in the conductive band should be much larger than the number for the associated valence band.

$$\alpha = \frac{\alpha_0}{1+S}$$

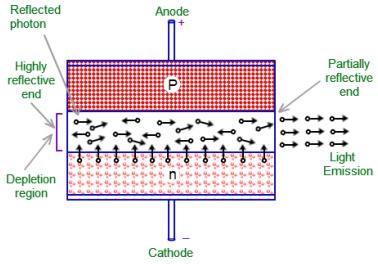


Figure 7: Laser diode. Adapted from [https://www.findlight.net]

## 1.15 Fabry-Perot Interferometer (FPI)

The FPI is a device allowing for selective transmission of a signal, depending on the wavelength. It consists of two highly reflective parallel surfaces at a distance of d from each other. If e consider an EM wave with frequency $\nu$ and the wavenumber $k = \frac{2\pi\nu}{c}$, the wave equation can be written as:

$$\phi(r,t) = U(r)exp(i\omega t)$$

We need the wave to fulfill the Helmholtz equation as well as the condition of disappearing at both edges of the interferometer: true only for resonant modes corresponding to resonant frequencies:

$$\frac{d}{\lambda_n} = 2n \Rightarrow \; k_n = \frac{2\pi}{\lambda_n} \Rightarrow k_n \cdot n = \frac{\pi n}{d}$$

Resulting in:

$$\nu_n = \frac{c}{\lambda_n} = \frac{nc}{2d}$$

The spacing between two adjacent resonant frequency modes- (FSR) Free Spectral Range- is equal to $\frac{(n+1-n)c}{2d} = \frac{c}{2d}$. After entering the FPI, as the wave gets reflected multiple times, its amplitude decreases upon each reflection by the factor of reflectivity- r. The phase difference between the original and each reflected wave is $\phi = 2dk$ since the wave needs to travel the distance d twice before returning to the incidence point.

From considering the geometric series for calculation of the total amplitude of interfering waves, we can measure the intensity- the square of the sum of the amplitudes. The final expression reads:

$$I = \frac{I_0}{(1-r)^2+4r\sin^2\left(\frac{\phi}{2}\right)} = \frac{I_{\max}}{1+\left(\frac{2\mathscr{F}}{\pi}\right)^2\sin^2\left(\frac{\phi}{2}\right)}$$

The $\mathscr{F}$ denotes the quantity of an interferometer called the 'finesse':

$$\mathscr{F} = \frac{\pi\sqrt{(r)}}{1-r} = \frac{\pi}{T+L}$$

The maximal intensity is equal to $I_{max} = \frac{I_0}{(1-r)^2}$. Finally, with the FSR denoted as $\nu_F$, a final expression for the FWHM of the intensity profile reads:

$$\delta\nu = \frac{\nu_F}{\mathscr{F}} \tag{21}$$

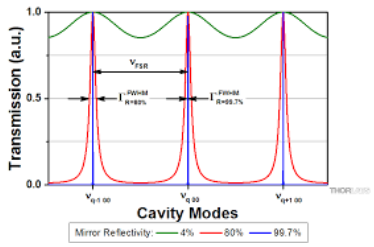


Figure 8: FPI cavity modes. Adapted from [https://www.findlight.net]

### 1.16 The procedure- Saturation Spectroscopy

1. Laser signal generation in the laser diode.
2. Signal passes a beam splitter.
3. One part is attenuated by an aperture and passes the FPI.
4. The second part is attenuated by a filter and passes another beam splitter.
5. Once the portion passes straight through and goes through the glass cell filled with rubidium gas (pump beam).
6. The second portion, reflected, is further attenuated by a filter, guided to mirror 2, and passes through the glass cell anti-collinearly.
7. Semi-transmissive mirror 1 guides the probe beam to the photodiode.
8. Two signals are recorded: the FPI transmission and that of absorption or saturation of the glass cell.

Absorption spectra is measured by putting a card at position W, blocking the beam.

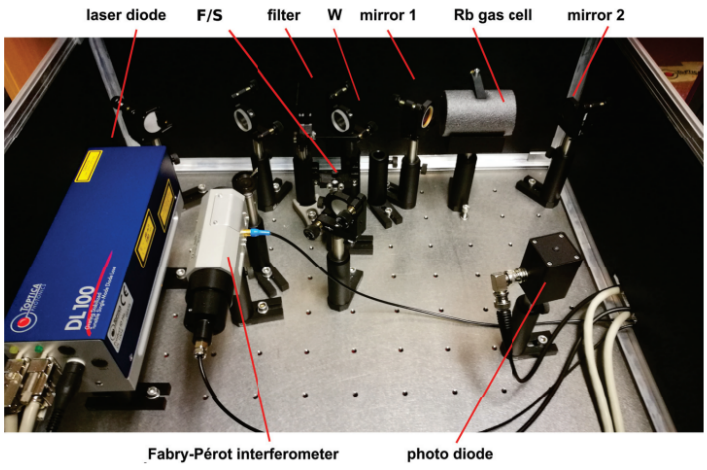


Figure 9: Experimental setup. Adapted from [1]

# 2 Tasks

## 2.1 Task 1

### 2.1.1 Scaling the Data

It is known that the spectral range of the FPI in our experimental setup is equal to $\Delta_{freq}$=1GHz. The spectral peaks can be plotted from the gathered data against the 'count'- our set scale of positive integers.

To know the correspondence of the 'count' scale to the real frequency distance, we can divide the peak-to-peak distances in both scales, one by another. This scale's unit will be further referred to as one count. The first difficulty arises when we realize that the peak-to-peak distances are not equal depending on the type (task) of measurement in question. For instance, the distances are equal to roughly 63 counts in Task 2 and 513 counts in Task 3. Therefore, we decide to carry the task out on a data set of task 4, since it will be useful later.

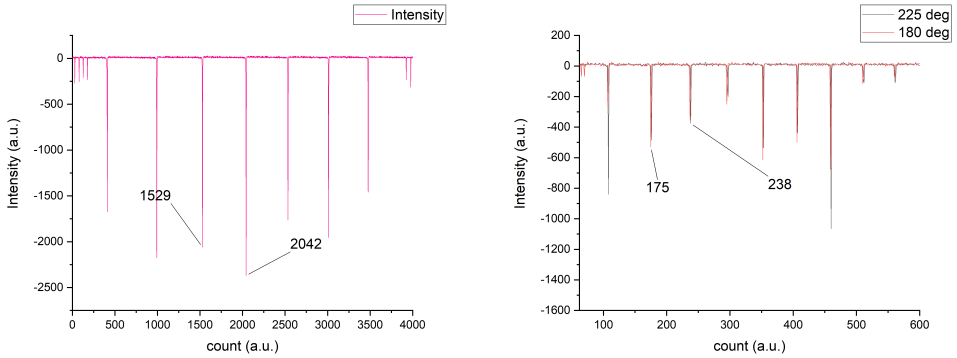


(a) Task 2 (b) Task 3

Figure 10: FPI spectrum measured for different tasks

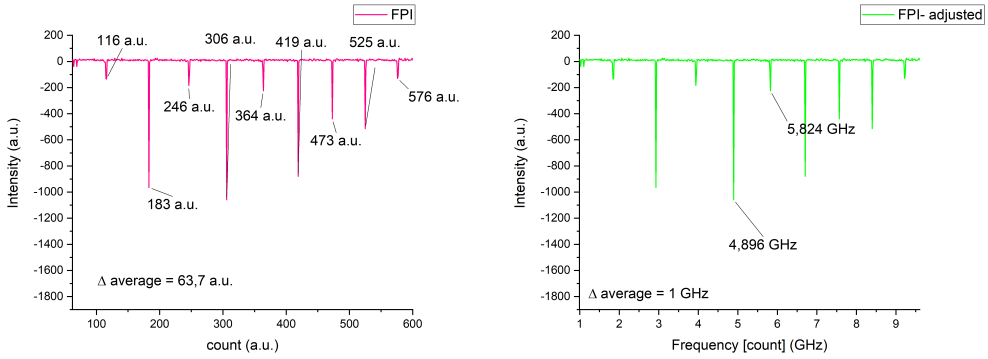


(a) Integers scale (count) (b) GHz adjusted scale

Figure 11: FPI peaks measured for task 4

For the chosen dataset, we find that the average peak-to-peak distance is equal to $\Delta_{freq} = 63{,}7$ counts. Hence, a distance conversion is assembled:

$$\frac{\Delta_{freq}}{\Delta_{count}} = \frac{1GHz}{63{,}7count} \approx 0,016\frac{GHz}{count}$$

### 2.1.2 Finding the finesse

Here, we use equation (21) to determine the finesse value with the previously found conversion. We need to know the FWHM, $\delta_\nu$ value for a single peak, which is found by fitting a Lorentzian profile to a singled-out FPI peak.

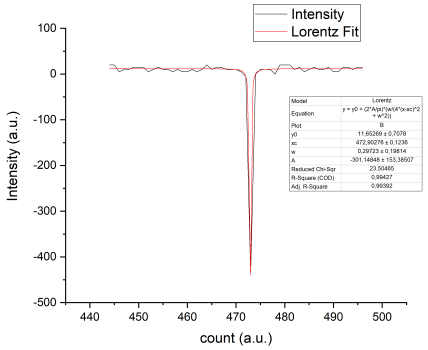


Figure 12: FPI peak measured for task 4 with fitted Lorentz distribution

From the fit, we obtain $\delta_\nu \approx 0,297$ counts. Together with the FSR=$\nu_F$ of 63,7 counts, we find:

$$\mathscr{F} = \frac{\nu_F}{\delta_\nu} = \frac{63{,}7}{0{,}297} = 214,48$$

## 2.2 Task 2

In this part, we attribute the frequency peaks of the rubidium spectrum to the correct isotopes in certain ground states. We know that in the isotopes mixture, the $^{8}7Rb$ comes in F=1 and F=2 ground states with the excited states F=0,1,2,3 while $^{8}5Rb$ comes in F=2 and F=2 ground states with the excited states F=1,2,3,4. Here, we focus on the $D_2$ line (780.2 nm) with transitions between $j = \frac{1}{2}$ and $j - \frac{3}{2}$, as shown in (Fig. 4).

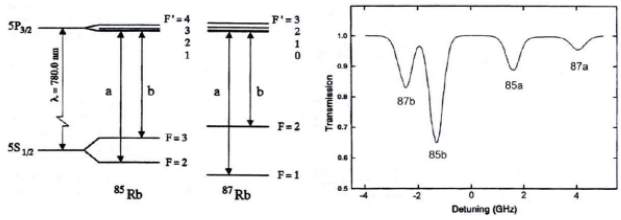


Figure 13: Hyperfine structure of Rubidium and transition lines. Adapted from [3]

Moving on, we have to assess the effect of a change in injection current and temperature of the diode. We plotted the saturation spectra accordingly, grouped by the applied injection current with varied temperatures. The first observation is the repeating peak pattern for every injection current and temperature setting. The repetition of the pattern happens approximately after the range of counts we presented in our graphs.
The effects the changes in the two factors have on the laser diode could be:

- **Mode Hopping** Single-mode laser's output switches between different longitudinal modes. In this context, the temperature or power (injection current) changes shift the wavelength of maximal gain [5]. A mixture of different frequencies emitted might occur right after the hopping before completely taking over the whole optical power of the diode by a mode different from the initial. This may lead to multiple different peaks and patterns arising at different temperatures and injection currents. Frequent mode hopping will show in an increased noise of a spectrum. Provided that the hopping is subtle, a more organized shifting of the whole spectrum could be observed (shift of the repeating pattern by a certain value). If the shift is close to a full wavelength/ multiple of the initial frequency, the change in spectrum may not be noticeable. As the emitted frequency will change, so will the intensity of the spectrum. Thus, we will look at abrupt changes in intensity or shifting of the spectral pattern in terms of mode hopping.

- **Change of the size of active region of the semiconductive laser diode** Increasing the temperature or the injection current (which is an indirect temperature change operation, since it leads to heat production) can change the wavelength emitted by the laser through a change. As the temperature rises, the semiconductor materials in the laser structure expand due to increased atomic vibrations. That expansion can slightly increase the dimensions of the active region, affecting the properties of the optical modes within the laser cavity.

- **Spectral Broadening** A direct or indirect change in temperature or the power (injection current) of the diode can influence the broadening of the spectra together with the carriers' average velocity.

First, we plotted two selections of spectra at fixed temperature with a variation of injection current (Fig. 6). Subfigure A shows a significant drop in spectral intensity as we change the current to 122 to 124 mA. An even more visible jump can be seen in Subfigure B upon change from I=105 mA to I=111 mA. Both of these changes could signify a mode jump. As expected, the spectral patterns change significantly upon the current variation. For subfigure A noise increase with higher currents can be seen. The spectral broadening aspect is not directly visible, but rather a repetition of similar patterns (I=105 mA similar to I=121 mA) shows in subfigure B which might signify a shift by close to full wavelength in laser emitted light.

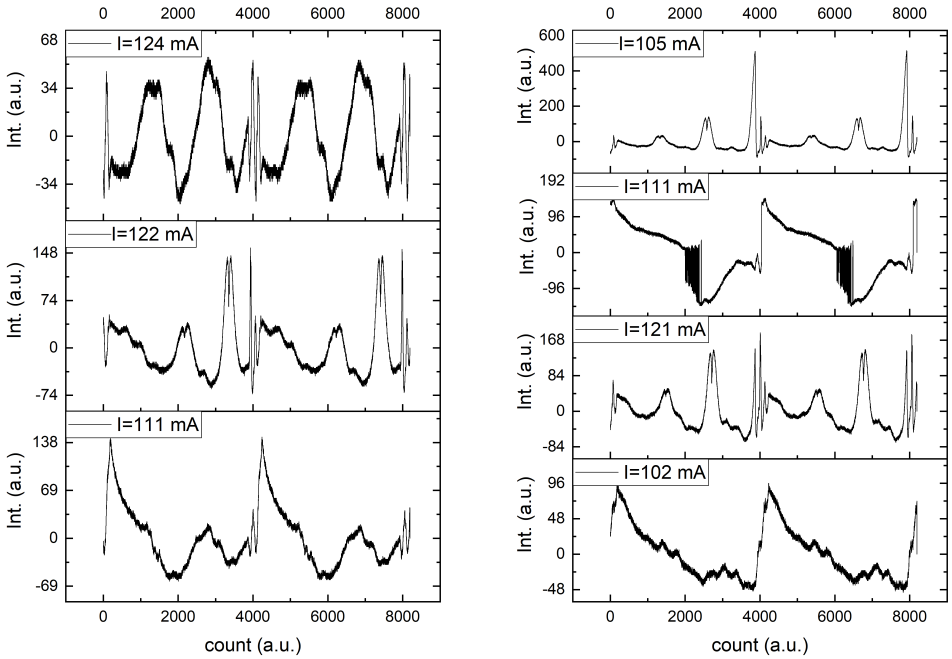


(a) Saturation spectra at 19.8 °C

(b) Saturation spectra at 20 °C

Figure 14: Saturation spectra for variation of injection currents

This time we will discuss the spectra obtained for a fixed current with temperature alteration (Fig. 7,8). First, we can observe a drastic increment in noise upon temperature increase (Fig.8, A). (Fig. 7 A) shows broadening for the spectra temperature increase with largely similar shape within the graphs set. The most homogeneous shape without a shift is kept in (Fig 8. B) with slight changes in resolution or appearance of occasionally added maxima. It could be caused by the fact that there is no mode jump between the measured spectra of that setting. The mode jumps occurred:

- between 20 °C and 20.2 °C for I=111 mA
- between 20 °C and 20.1 °C for I=121 mA

- between 19.8 °C and 20.1 °C for I=122 mA

Interestingly, the previously mentioned gradual shift of the spectral pattern is visible between graphs for 19.9 °C-20 °C and 20.1 °C-20.2 °C with peaks moving slightly towards the smaller values of [count].

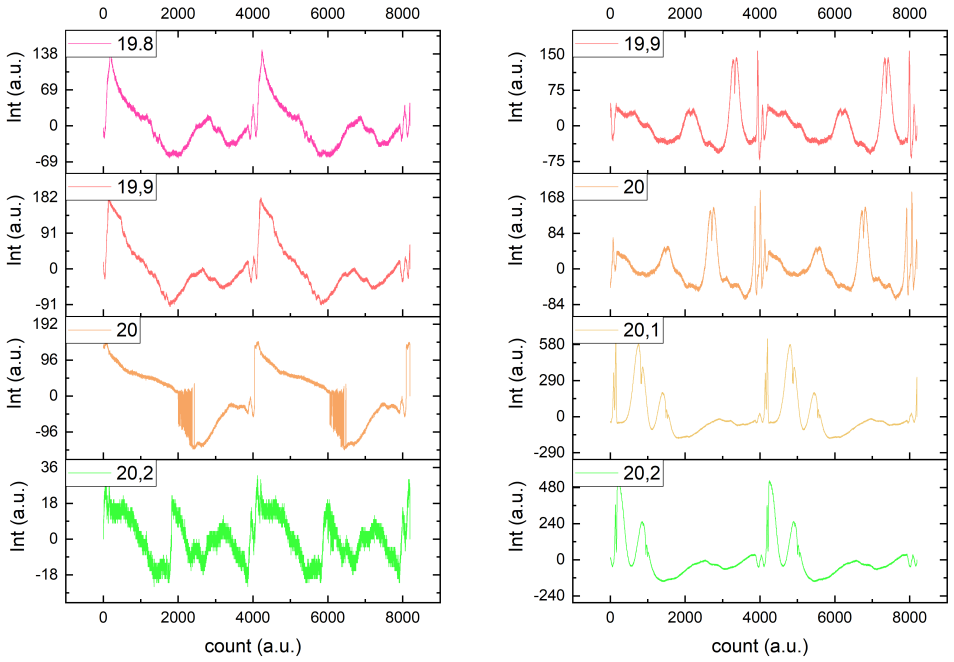


(a) Saturation spectra for I=111 [mA]

(b) Saturation spectra for I=121 [mA]

Figure 15: Saturation spectra for variation of currents

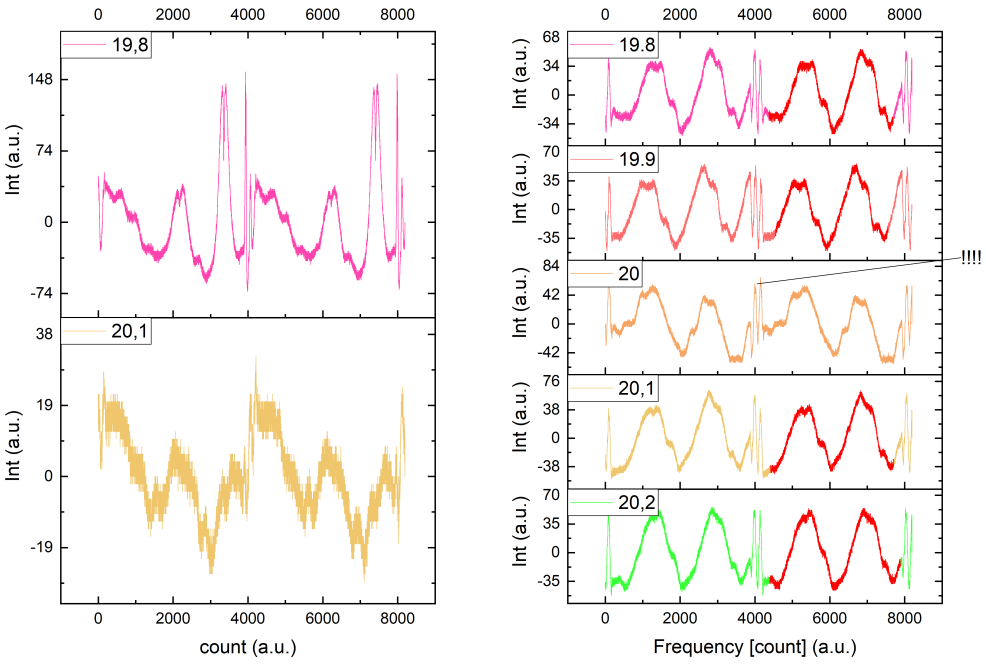


(a) Saturation spectra for I=122 [mA]

(b) Saturation spectra for I=124 [mA]

Figure 16: Saturation spectra for variation of currents

## 2.3 Task3

Next, we want to investigate the effect of replacing the regular filter with a gradient filter set to different positions. With increasing degree of rotation of the gradient filter wheel, the attenuation changes as the gradient gets more saturated. We measured the saturation spectra at different rotations (Fig. 7).

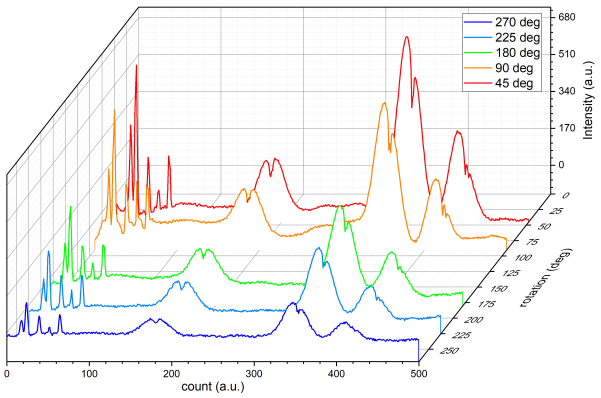


Figure 17: Saturation spectra measured at different rotations of the gradient filter

As we observe, increasing the darkness of the gradient happens as we rotate it by a larger angle. Hence, the spectra for larger rotation settings show larger intensity attenuation. We did not notice any change in peak positions. This result was expected, as there is no other interaction between the filter and the light than absorption or reflection of the beams. Thus, the same observation would arise for absorption spectra.

## 2.4 Task 4

*Fit the peaks in the absorption spectrum with a suitable fitting function. Extract the characteristics of the individual peaks and compare them with literature values.*

First, we plotted the absorption and saturation spectra alongside the difference between them (Fig. 8).

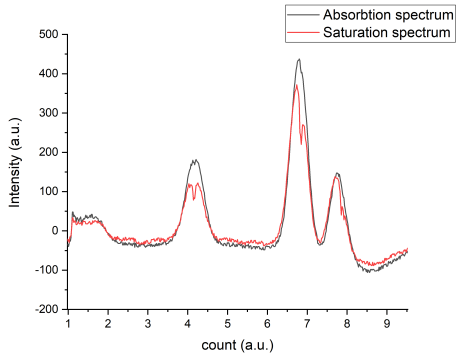


(a) Absorption and saturation spectra

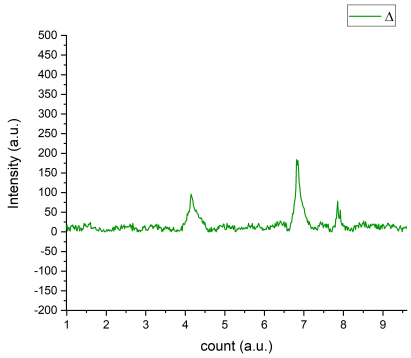


(b) Difference in intensities of the spectra

Figure 18: Full spectrum

We identified the peaks with energy levels, ${}^{8}7Rb_1$, ${}^{8}5Rb_2$, ${}^{8}5Rb_3$, and ${}^{8}7Rb_2$ from left to right, respectively. By marking the distances between particular peaks, in reference to [1], we complete the error analysis as follows:

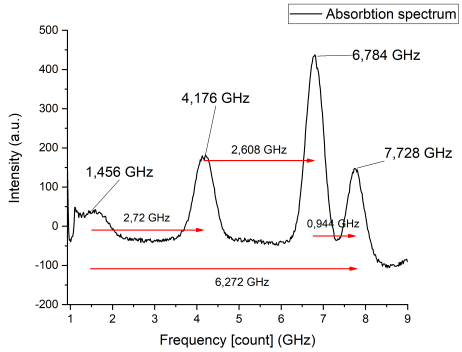


(a) Hyperfine spectrum peaks at ground state for Rubidium

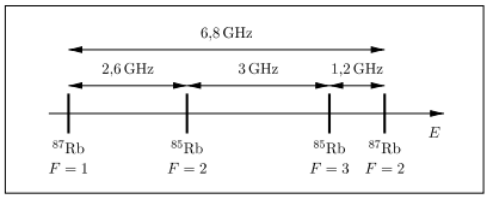


(b) Reference [1]

Figure 19: Full spectrum- distances

| Peaks | Distance exp (GHz) | Distance theory (GHz) | percentage error |
|---|---|---|---|
| ${}^{8}7Rb_1$ -${}^{8}5Rb_2$ | 2,720 | 2,5 | 8% |
| ${}^{8}5Rb_2$ -${}^{8}5Rb_3$ | 2,608 | 3 | 13% |
| ${}^{8}5Rb_3$ -${}^{8}7Rb_2$ | 0,944 | 1,3 | 27% |
| ${}^{8}7Rb_1$ -${}^{8}7Rb_2$ | 6,272 | 6,8 | 8% |

The comparison shows that we consistently obtained percentage errors exceeding the 5% threshold. The source of the error could probably be the calibration issue, since the previously determined value was the average, while overall peak distances tend to deviate. Next, we want to compare the quantity of the FWHM

of peaks fitted with the Voigt profile to the theoretical value of $\delta_\nu = 512MHz$ given as a theoretical prediction for 'Doppler width' in [3]. We extracted the values seen in the table below. The experimentally obtained FWHM values should be calculated with the found parameters by means of the formula from Kielkopf [REFERENCE]:

$$\omega_v \approx 0,5343\,\omega_L + \sqrt{0,2169\,\omega_L^2 + \omega_G^2}$$

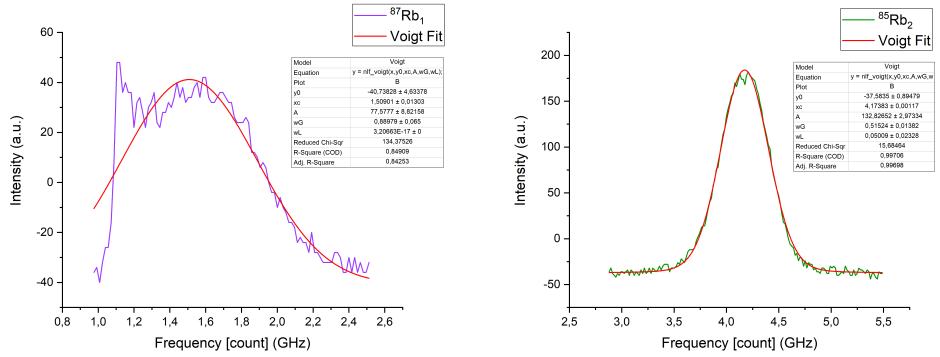


(a) $^{87}Rb_1$ (b) $^{85}Rb_2$

Figure 20: Spectrum peaks with Voigt fit

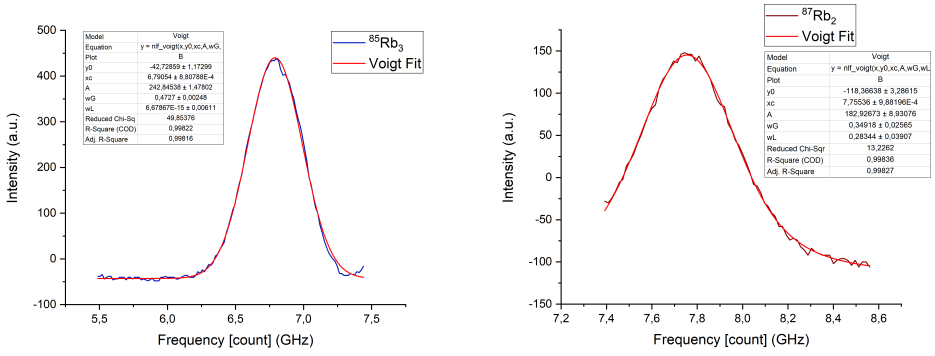


(a) $^{85}Rb_3$ (b) $^{87}Rb_2$

Figure 21: Spectrum peaks with Voigt fit

| Peak | FWHM exp (GHz) | FWHM theory (GHz) | percentage error |
|---|---|---|---|
| $^{8}7Rb_1$ | 0,89 | 0,512 | 74% |
| $^{8}5Rb_2$ | 0,54 | 0,512 | 5% |
| $^{8}5Rb_3$ | 0,47 | 0,512 | 8% |
| $^{8}7Rb_2$ | 0,53 | 0,512 | 4% |

As we can see, the error was relatively low (close to the acceptable threshold) except for the $^{8}7Rb_1$ peak, which is probably too noisy for correct fitting.

## 2.5 Hyperfine spectrum-excited states

*Assign the visible peaks and lamb dips using appropriate literature (e.g. [12]) to the corresponding hyperfine structure transitions of the D2 line. Compare their distance and spectroscopic characteristics with literature values (e.g. in [3],[4],[13])*

For the last task, we plotted the saturation spectra and assigned their dip values to hyperfine structure transitions of the D2 line. We used (3) for the comparison.

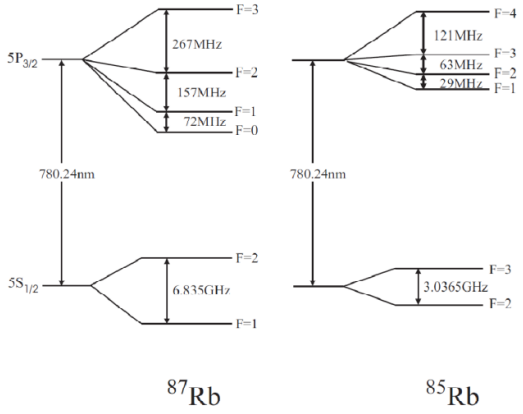


Figure 22: Hyperfine structure transition lines [3]

Additionally, we considered the so-called 'cross-over' frequencies. From [8] we read:

*"If the laser frequency is halfway between two atomic resonances, atoms with exactly one velocity class are on resonance for the pump and probe beam. However, the resonance condition for the two contra-propagating beams is fulfilled for different atomic transitions. This frequency is the Cross-Over-Frequency."*

The cross-over frequency is found as the average of two frequencies.

Now, we proceed to analyze the peaks one by one.

---

$^{87}Rb_1$

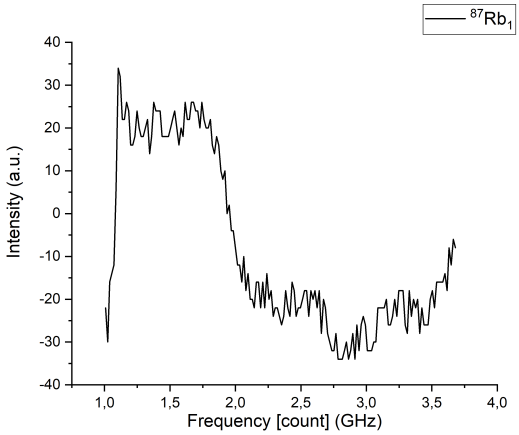


Figure 23: $^{87}Rb_1$

This plot was too noisy to find the characteristic dips. Thus, no analysis could be performed.

---

The plots for the rest of the peaks are much clearer. We identified the dips corresponding to standard and cross-over frequencies (here marked by $C_{ik}$) for the latter peaks. Then the measured distances between the dips were compared to those established from the theory [3], as shown in the figures below the particular spectra.

---

$^{85}Rb_2$

| $\Delta_{freq}$ | $\Delta_{freq}$ exp (MHz) | $\Delta_{freq}$ theory (MHz) | percentage error |
|---|---|---|---|
| F1 - F2 | 32 | 30 | 6,67% |
| F2 - F3 | 64 | 63 | 1,59% |

---

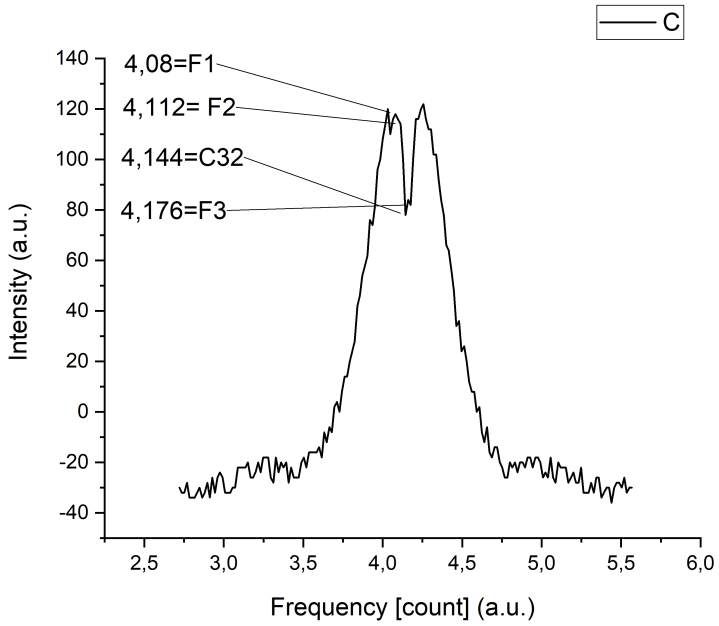


Figure 24: $^{85}Rb_2$


Figure 25: Hyperfine splitting

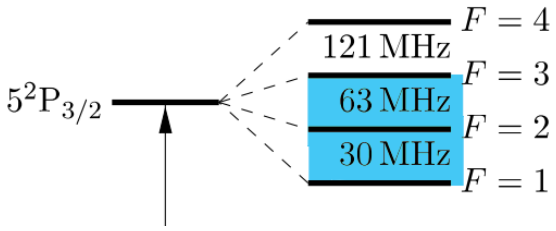


Figure 26: Cross-over frequencies distances. (Illustrative: the frequencies from Fig. 14 were used for comparison)

$^{85}Rb_3$

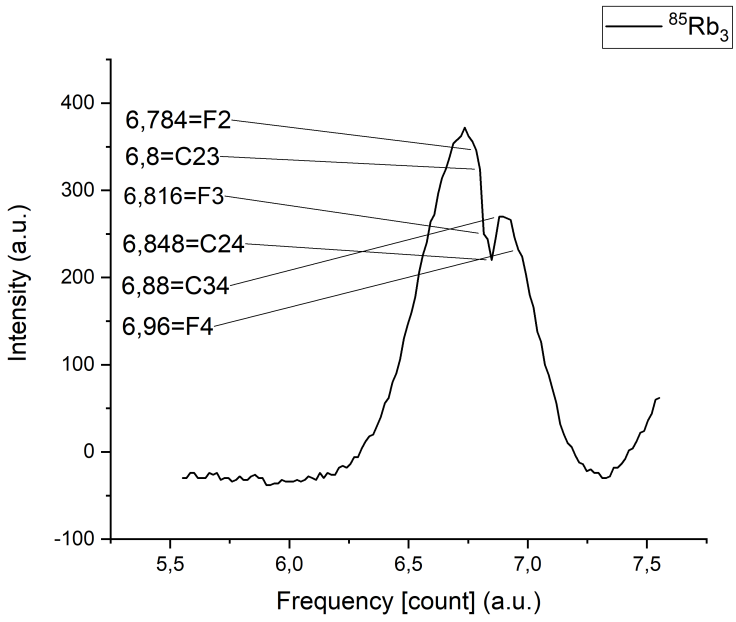


Figure 27: $^{85}Rb_3$

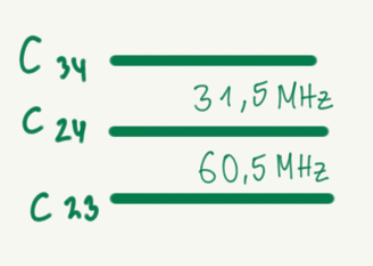


Figure 28: Hyperfine splitting

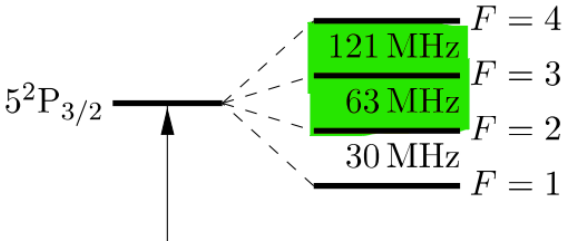


Figure 29: Cross-over frequencies distances. (Illustrative: the frequencies from Fig. 14 were used for comparison)

| $\Delta_{freq}$ | $\Delta_{freq}$ exp (MHz) | $\Delta_{freq}$ theory (MHz) | percentage error |
|---|---|---|---|
| C23 - C24 | 48 | 60,5 | 20,66% |
| C24 - C34 | 32 | 31,5 | 1,59% |
| F2 - F3 | 32 | 63 | 49,21% |
| F3 - F4 | 144 | 121 | 19% |

$^{85}Rb_3$

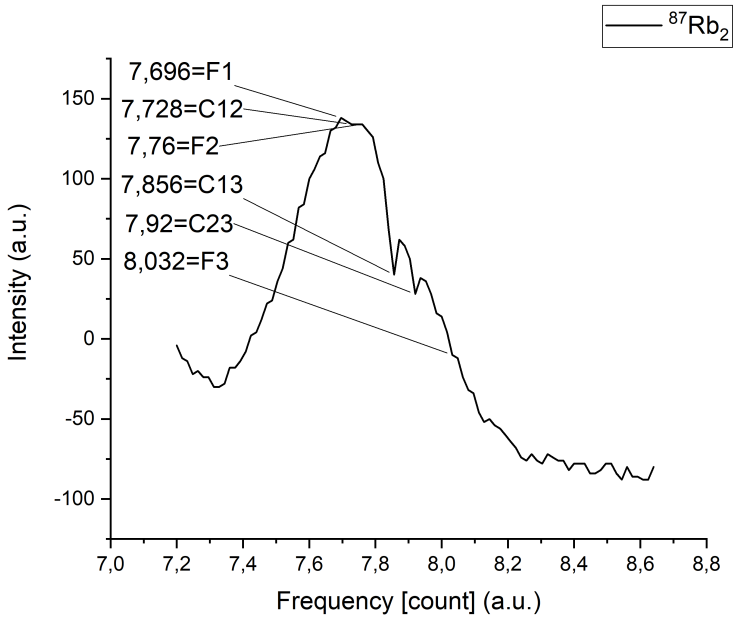


Figure 30: $^{87}Rb_2$


Figure 31: Hyperfine splitting

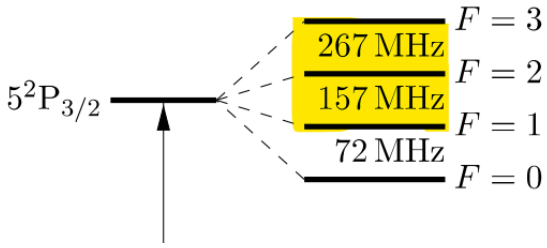


Figure 32: Cross-over frequencies distances. (Illustrative: the frequencies from Fig. 14 were used for comparison)

| $\Delta_{freq}$ | $\Delta_{freq}$ exp (MHz) | $\Delta_{freq}$ theory (MHz) | percentage error |
|---|---|---|---|
| C12 - C13 | 128 | 133,5 | 4,12% |
| C13 - C23 | 64 | 78,5 | 18,47% |
| F1 - F2 | 64 | 157 | 59,24% |
| F2 - F3 | 272 | 267 | 1,87% |

For most the assessed frequency distances, the values of the percentage error exceeded the 5 % range. This could again be due to a calibration problem of taking an average of all FPI peak distances.

---

## 2.6 Conclusions

In the process of completing the experiment, I learned about the laser spectroscopy method and its Doppler-free corrected version. I got to know the working principles of the setup and practised taking measurements. I believe the experiment's results were rather illustrative and provided an introduction to the topic. I managed to get a finesse value within the usual range found for comercial FPIs. The rough description of behaviour of the spectra in different settings reveals the broad issue of errors in spectroscopy. I completed fitting the voigt profiles and measuring hyperfine spectrum characteristics with a very restricted accuracy. The learning principle of the experiment remains fulfilled.

## 2.7 References

1.Demtroder Laser Spectroscopy 1
2.Manual Advanced Laboratory
3.https://physics.unm.edu/ Courses/Drake/Phys493LSp21/LabGuides/satabs2.pdf
4.John F. Kielkopf: New approximation to the Voigt function with applications to spectral- line profile analysis. 8. Auflage. Vol. 63. Journal of the Optical Society of America, 1973.
5.https://www.rp-photonics.com/mode-hopping.html
6.Solid-state 13 C NMR of carbon nanostructures (milled graphite, graphene, carbon nanotubes, nanodiamonds, fullerenes) in 2000–2019: a mini-review, A Mazur

7.https://www.physics-and-radio- electronics.com/ physics/laser/ methodsofachievingpopulationinversion.html

8.https://www.physik.hu-berlin.de/en/qom/ lehre/f-praktikum-laserspektroskopie/anleitung.pdf